



ORIGINAL RESEARCH ARTICLE

Increasing Energy Efficiency by Optimizing Heat Treatment Parameters for High-Alloyed Tool Steels

Jannik Schuppener , Santiago Benito , and Sebastian Weber

Submitted: 5 January 2024 / Revised: 12 March 2024 / Accepted: 28 March 2024

In the paper industry, machine circular knives are used in the cutting process to provide industrial quality cuts on a variety of products. In the production of paper rolls, they cut the long-rolled paper products into commercial sizes. For this application, the high-alloyed ledeburitic cold work tool steel, DIN EN 1.2379 (X153CrMoV12; AISI D2), in the secondary hardened heat-treated condition has become the widely used industry solution. However, its heat treatment is a very energy-intensive production process. It consists of a quenching from an austenitizing temperature above 1050 °C, followed by three high-temperature tempering steps of more than 500 °C. In the study, the heat treatment process was optimized for energy efficiency, resulting in superior material properties with lower energy consumption. The most promising low energy heat treatment developed in the laboratory was reproduced in the industrial scale, and the required energy consumption was quantified. Subsequently, the resulting properties of the tools such as hardness, wear resistance and fracture toughness were determined. The energy production costs and mechanical properties of the tool steel were evaluated in comparison to conventional production methods. The newly applied heat treatment condition showed very promising and positive results in all analyzed parameters.

Keywords energy efficiency, heat treatment, optimization, tool steel

1. Introduction

The efficient production of high-quality tool steels plays a central role in our global manufacturing landscape, as they process steels or other materials and components of varying size and complexity. As pointed out by Berns and Theisen (Ref 1), these tools require mechanical strength, hardness, wear resistance and a balanced level of toughness. The intricate interplay of these properties is attributed to the multi-phase microstructure of the tool steels, a property that is meticulously tailored through a combination of manufacturing processes, chemical composition adjustments and careful heat treatments, as elucidated by Hornbogen et al. (Ref 2). In particular, Bhadeshia and Honeycombe (Ref 3) emphasize that each facet of this microstructure contributes significantly to the final macroscopic properties of the tools.

Today, given the need for sustainable practices and resource optimization, we must find new ways to reduce energy consumption, such as in energy-intensive heat treatment processes. If the quality of the tools is not compromised in the process, this can lead to cost savings and environmental benefits (Ref 4). Therefore, it is crucial to explore energy-

saving methods during the heat treatment process and to review old conventional processes (Ref 5). In addition, improving material properties while reducing environmental impact is always a goal of future industrial development. After all, the heat treatment parameters used are generally not designed with all variables in mind. Rather, they are the result of trial and error, based more on tradition than on knowledge of the process-structure-property chain.

Machine circular knives are used in the paper industry to precisely cut a variety of products. These knives ensure high-quality industrial cuts. Specifically, for the production of paper rolls, they are used to cut long-rolled paper products into commercial sizes. The making of these top-notch tools requires many high-precision thermal and mechanical production steps. TKM GmbH, headquartered in Remscheid, Germany, is the world's leading supplier of machine circular knives in this field. These are used in the metal, paper and wood industries. For this application, the high-alloyed ledeburitic cold work tool steel DIN EN 1.2379 (X153CrMoV12; AISI D2), in the secondary hardened heat-treated condition has become the de-facto industry solution. In the production, TKM receives circular plates that have been laser-cut from a flat material and feature a central bore made of cross-rolled AISI D2 steel. The blanks are typically 610 mm in diameter and 5.6 mm in thickness (Ref 6). The next stage in production is the energy-intensive heat treatment, which has multiple stages. First, hardening the blanks at a temperature above 1050 °C takes place in a gas-heated industrial continuous furnace. Then, contact quenching between two forging punches follows. Afterward, the circular knives are stacked in four packs, each containing 75 knives, and tempered three times at 510 °C in an electrically heated forced-air furnace. Due to the high volume of the stacks, this tempering process can take up to 70 hours in total. Because of the heat treatment required to adjust the properties of the

Jannik Schuppener, Santiago Benito, and Sebastian Weber, Chair of Materials Technology, Ruhr-University Bochum, Universitätsstraße 150, 44801 Bochum, Germany. Contact e-mail: Schuppener@wtech.rub.de.

material, a large amount of combustion gas is required for the industrial continuous furnace, and a large amount of electricity is required for the electrically heated tempering furnaces. After heat treatment, the next production steps are surface grinding, grinding to the cutting geometry, tension rolling, surface polishing, straightening and subsequent sharp grinding and quality control.

In this work, an alternative, more energy-efficient heat treatment was developed, taking into account the required quality characteristics of the circular knives. For this purpose, a possible alternative heat treatment was first investigated and developed on a laboratory scale (section 3.1). The most promising alternative heat treatment was then reproduced industrially (section 3.2). The required energy consumption was measured and compared to the conventional production route. In addition, the microstructure of the two industrial heat treatment routes and their main mechanical properties, such as hardness, toughness, and abrasive wear resistance, were compared.

2. Experimental

2.1 Sample Geometry, Material Used and Preparation

In this work, a disk with a diameter of 61 mm and a thickness of 5.6 mm (Fig. 1 a) made of the a ledeburitic cold work steel DIN EN 1.2379 (X153CrMoV12; AISI D2) was used to optimize the heat treatment in the laboratory furnace. The as-received condition was soft annealed. The chemical composition was analyzed by optical spark emission spectrometry (OES) and the mean value from five individual measurements is shown in Table 1. The used disk is a center cutout part of one real circular knife (Fig. 1a). The disk was sliced into $10 \times 10 \times 5.6$ mm cubes for each anticipated heat treatment phase. Afterward, we performed the heat treatment detailed in

section 2.2.1, followed by an analysis of mechanics and microstructures (refer to sections 2.3 and 2.4.1).

2.2 Heat Treatment and Temperature Measurement

2.2.1 Laboratory Furnaces. The heat treatment of the disks pieces was carried out in a laboratory muffle furnace in an argon atmosphere followed by quenching in oil. The austenitizing temperatures were chosen between $T_A = 950\text{--}1055$ °C and the total heat treatment time for each temperature was $t_A = 30$ min (Table 2). This heat treatment variation was selected to achieve the maximum possible hardness through the austenitizing temperature after quenching. To ensure a uniform temperature distribution in the laboratory furnace, it was preheated to the austenitizing temperature for two hours. After preheating the furnace, the metallic sample was placed in the furnace and then the actual heat treatment of the samples took place. For each austenitizing temperature, successive tempering was performed in a temperature range from room temperature to 240 °C for 120 min for each temperature step (Table 3), followed by cooling in air. A schematic representation of the heat treatment performed in the laboratory furnaces using the parameters listed in Table 2 and 3 is shown in Fig. 2.

2.2.2 Quenching Dilatometry. A quenching dilatometer DIL805 (TA Instruments, DE, USA) was used to measure the M_s temperature after different heat treatments. For the experimental determination of the M_s temperature, cylindrical dilatometer specimens with a diameter of $D = 4$ mm and a length of $L = 10$ mm were made from the same material mentioned in section 2.1. The austenitizing temperature was varied between $T_A = 980\text{--}1100$ °C and the holding time was between $t_A = 1\text{--}60$ min. Al_2O_3 punches were used to measure the change in length of the specimens, and 0.1 mm diameter S-type thermocouples were welded to the surface of the dilatometer specimens for temperature measurement and control. To reduce oxidation, the tests were performed under vacuum ($\sim 5 \times 10^{-4}$ mbar) followed by quenched with N_2 . In

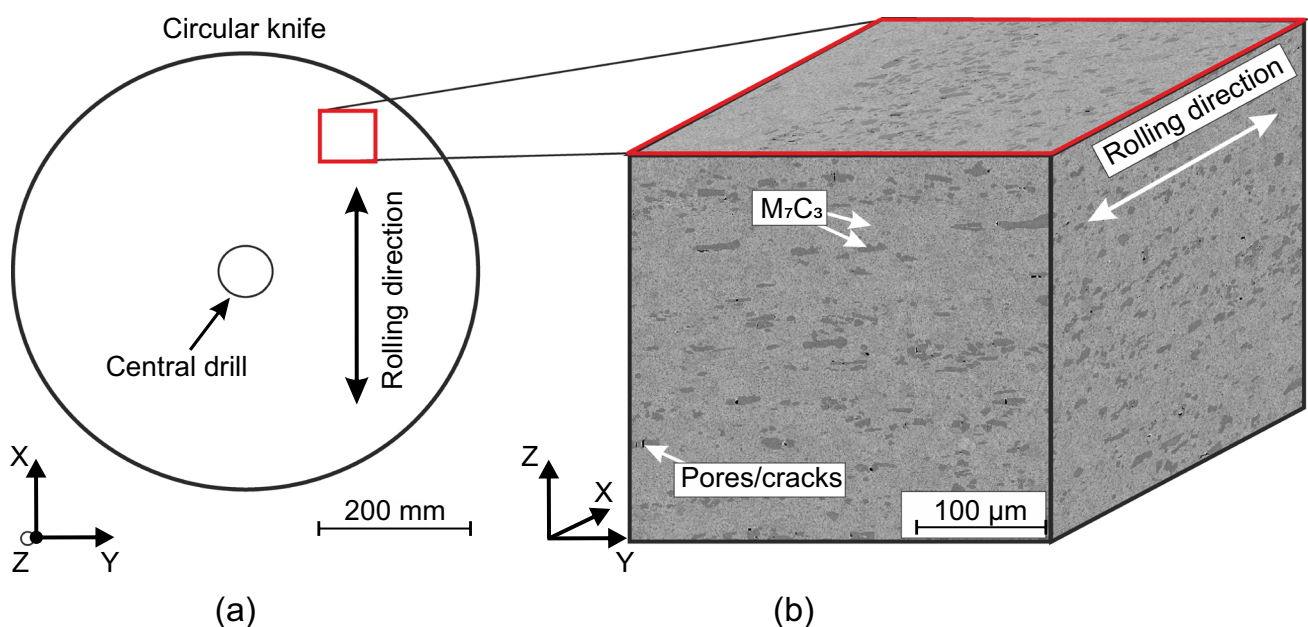


Fig. 1 Schematic sketch (a) of the examined circular knife with the cutout central drill for the laboratory heat treatment investigations. 3D microstructural image (SEM with SE contrast) of eutectic M_7C_3 carbides aligned by the rolling process in the as-delivered condition (b)

Table 1 Chemical composition of the steel 1.2379 (AISI D2) determined by optical spark emission spectrometry (OES) in wt.%

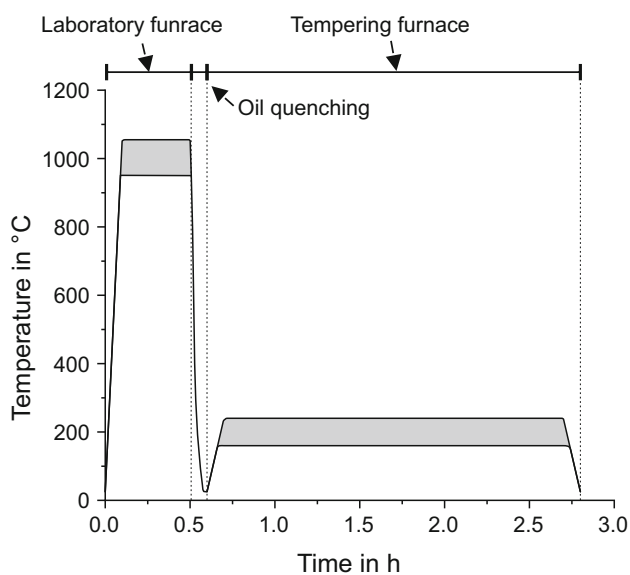
Element	C	Si	Mn	P	S	Cr	Ni	Mo	Cu	V	W	Co	Fe
wt.%	1.592	0.34	0.38	0.02	0.01	11.29	0.19	0.73	0.06	0.56	0.09	0.02	bal.

Table 2 Selected austenitizing temperature ($t_A = 30$ min) for the optimization of the heat treatment in the laboratory furnace

Austenitizing temperature T_A in °C	950	970	980	990	1010	1020	1055
---------------------------------------	-----	-----	-----	-----	------	------	------

Table 3 Selected tempering temperature ($t_{Temp} = 120$ min) for optimizing heat treatment in the laboratory furnace for each austenitizing temperature in Table 2

Tempering temperature T_{Temp} in °C	25	160	180	200	220	240
--	----	-----	-----	-----	-----	-----

**Fig. 2** Schematic representation of the heat treatment performed in the laboratory furnaces using the parameters listed in Tables 2 and 3

the experimental variation of the austenitizing temperature between $T_A = 980$ – 1100 °C, the mean quenching rate was -40 ks^{-1} . The experimental optimization of the industrial heat treatment parameters in the dilatometer (section 3.1.2) achieved the same heating and cooling rates as in the industrial continuous furnace. The second derivative of length change versus temperature was examined to evaluate the dilatometer data.

2.2.3 Industrial Heat Treatment. Once the new energy-efficient heat treatment parameters were found on a laboratory scale, their functionality was tested on an industrial scale. Austenitizing was carried out for each individual circular blade in a continuous roller furnace from WMU GmbH. A schematic illustration of the continuous furnace is shown in Fig. 3. Five heating zones of different lengths can be individually con-

trolled. For this purpose, Type S thermocouples are used, which are labeled T_1 – T_5 in the figure. In the first section of the furnace, a constant slow throughput speed of 350 $mm\ min^{-1}$ (V_1) is selected to achieve the required heat treatment time in the furnace. The subsequent speed V_2 is 8500 $mm\ min^{-1}$ to transfer the circular knives to the following production step. With the temperature settings and throughput speed, a time-temperature curve of the actual heat treatment of the circular knives can be obtained.

A GRAPHTEC GL240 series data logger, specifically a GL240 midi LOGGER, was used in connection with Type S thermocouples to measure the temperature in the heat treatment. To measure the temperature inside the continuous furnace, a thermocouple was attached to a circular knife positioned approximately 2 cm above the conveyor rollers to facilitate temperature detection. Simultaneously, a second thermocouple was inserted into a lateral bore, extending to a depth of 2 cm within the circular knife, to measure the resultant temperature within the knife itself.

The subsequent quenching is carried out between two forging punches cooled to 35 – 60 °C (Fig. 4a). The circular knives need to reach a temperature below 60 °C. This cooling process requires a cooling time of 150 seconds, allowing a maximum production speed of 24 cooling cycles per hour, or 48 standard-sized circular knives.

After quenching, depending on the thickness of the circular knives, up to 75 pieces (with $D = 5.6$ mm) are screwed between two metal blocks and clamped by contact pressure, as shown in Fig. 4(b). Both the quenching between two forging punches and the clamping of the round packs for the subsequent tempering process in the tempering furnace are used to minimize distortion of the semi-finished products during heat treatment. Four of these stacks are heat treated simultaneously in a tempering furnace, resulting in a quantity of $n = 300$ pieces per furnace for the standard circular knives.

During the tempering heat treatment, a groove with the diameter of the thermocouple was milled in the center circular blank in the stack ($N = 38$) so that a thermocouple could be placed up to the center hole and fixed to the center of the

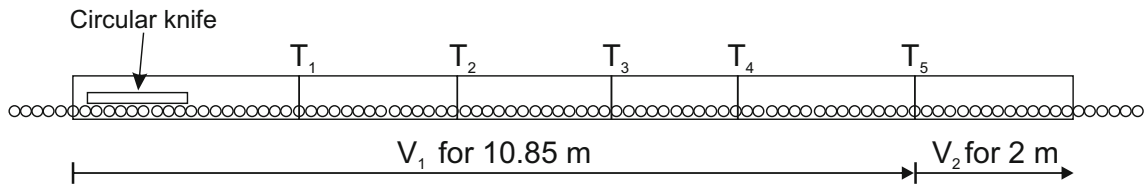


Fig. 3 Schematic illustration of the used industrial continuous furnace from WMU GmbH. T_1 – T_5 are the positions of the thermocouples for controlling the furnace temperature, and V_1 and V_2 are the freely adjustable throughput speeds

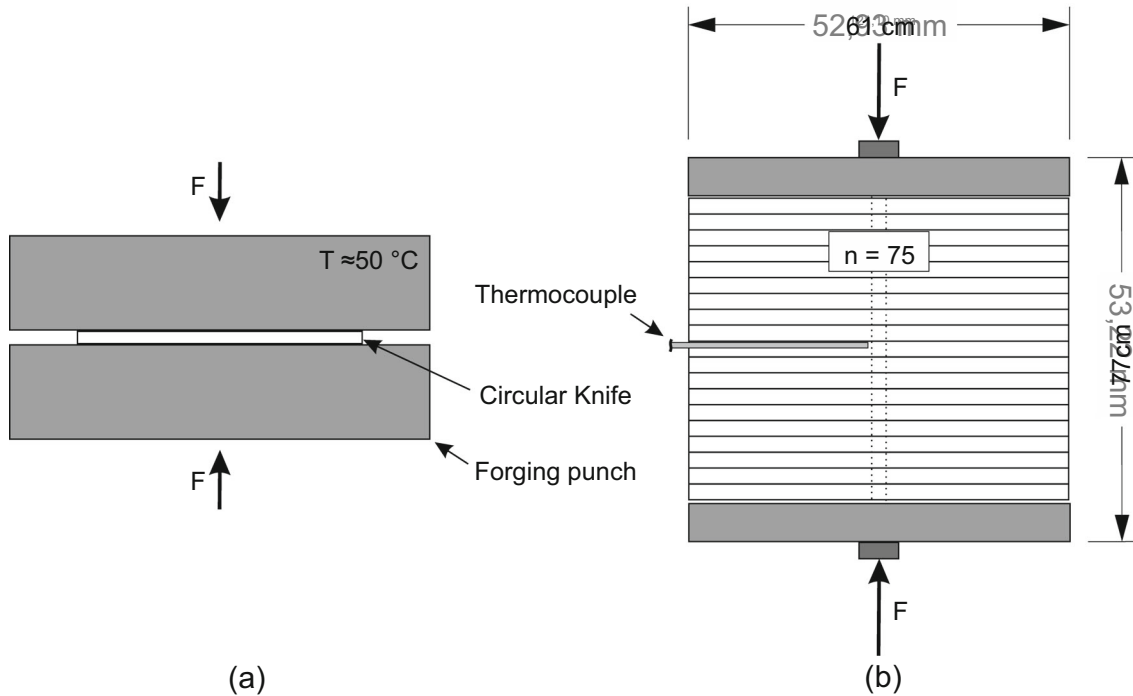


Fig. 4 Illustration of industrial quenching after austenitizing between two cooled forging dies (a) and stacking of circular knives for tempering (b). Both processes shown are used to minimize distortion during heat treatment

circular knife stack. The furnace temperature was also measured by placing a second thermocouple at the same height as the first, next to the circular knife stack.

2.3 Microscopy and Quantitative Phase Analysis

The metallographically prepared specimens underwent microstructural and phase analysis. To do this, the metallic samples for examination were hot embedded individually in conductive material, and then metallographically ground and polished using 1 μm diamond suspension. For high-resolution imaging of microstructures, we utilized a TESCAN GmbH MIRA3 scanning electron microscope (SEM) with an acceleration voltage ranging between 15 kV and a working distance of 10 mm. To conduct quantitative image analyses, the BSE detector was used on polished samples. The local chemical composition was analyzed using energy-dispersive x-ray spectroscopy (EDS) with a 20kV acceleration voltage, a working distance of 15 mm, the Xman-detector, and the evaluation software AZtec (Oxford Instruments, United Kingdom). Electron backscatter diffraction (EBSD) was used for phase identification, with an acceleration voltage of 20 kV, a working distance of 17 mm, a step size of 0.11 μm , and an electron beam spot size of 0.04 μm . For EBSD analysis, the samples

were further deformation-free polished for 12 h on a QATM Saphir Vibro vibratory polisher using a chemo-mechanical oxide polishing suspension (OPS). The EBSD scans were conducted using the Nordlys Nano Detector and AZtec software from Oxford Instruments on tilted specimens at a 70° angle. Phase identification of α -Fe, γ -Fe, M_7C_3 , M_3C , M_3C_2 and M_2C was accomplished utilizing the inorganic crystal structure database (ICSD). Subsequently, the specimens underwent etching with V2A acid (100 ml H_2O + 100 ml HCl + 10 ml HNO_3), and microstructure images were generated with SE contrast.

2.3.1 Image Analysis. For the quantitative measurement of the carbide content, we utilized image analysis. In this study, we captured 64 individual images per sample using a magnification of 15 kx and a square image side length of 18.4 μm . Brightness, contrast and working distance remained consistent between different specimens. The individual images were combined to create a panorama image for each sample utilizing the Fiji ImageJ2 1.52p software (Ref 7). The method was repeated three times for each specimen, and three large high-resolution images were evaluated. A custom developed software created by Benito et al. (Ref 8) was utilized in MATLAB® for a two-stage semi-automatic segmentation

process of quantitative image analysis that involved both gray level and feature size thresholding. The identified phases were identified based on their properties such as contents, individual feature sizes, and shapes, all of which were determined using area fraction, equivalent diameter, and aspect ratio descriptors.

2.3.2 X-Ray Diffraction. Quantitative phase analysis of retained austenite was performed on the metallographically polished specimens using the PULSTEC μ -X360n mobile x-ray diffractometer, which uses Cr x-ray ($\text{CrK}\alpha$ radiation; $\lambda = 0.22898$ nm) with 30 kV voltage and 1 mA current. The largest collimator (2 mm aperture) was used, and the x-ray exit-to-sample distance was 20 ± 0.5 mm. An 18° beam entrance angle (ψ_0) resulted in an oval irradiated measurement range of 3.0×2.8 mm on the specimen. The XRD detected the diffraction of γ -iron (retained austenite) in [220] orientation and α -iron (martensite) in [211] orientation. The quantitative phase ratio between γ - and α -iron was calculated from the integrate intensities of both phases according to (Ref 9) for the x-ray determination of retained austenite. An average of at least five measurements was taken for each heat treatment variation, with a sample rotation of 60° between each measurement. The same method was used for the wear specimens in section 2.4.2 to investigate the deformation induced transformation of the retained austenite. For this purpose, a metallographic sample polished to $1 \mu\text{m}$ was measured and assumed to be deformation free. Then, after the wear tests, the retained austenite content was measured by x-ray in the wear track and compared with the deformation-free retained austenite content.

2.4 Mechanical Properties

2.4.1 Hardness Testing. The hardness of the metallographically prepared samples was measured using the Vickers method (DIN EN ISO 6507) in HV10. HV10 corresponds to a test load of 98.08 N applied to the specimen surface with the Vickers indenter (straight pyramid) for 10 seconds. For each measuring point, a minimum of five individual measurements were carried out on a hardness tester from KB Prüftechnik GmbH, and the arithmetic mean and standard deviation were calculated. The hardness of the tool was the main optimization parameter, which must be between 700 and 750 HV10 to achieve the required product quality of the circular knives from TKM GmbH.

2.4.2 Impact Toughness. Impact toughness was tested on samples stemming from the industrial production. Since the initial material of the circular knives is only about 5.6 mm thick, it was not possible to produce specimens according to the standard ($10 \times 10 \times 55$ mm). The specimens used for the toughness test had a specimen geometry with dimensions of $5 \times 10 \times 55$ mm without notch, which is an “undersize specimen” according to the standard DIN EN ISO 148-1:2016 (Ref 10). Thus, the analyzed values can only be compared to literature values obtained with the same sample size. To minimize the influence of surface defects due to the mechanical fabrication of the specimens, the tensile loaded surface (5×55 mm) was polished without scratches to a grain size of $1 \mu\text{m}$ diamond suspension. Impact toughness was performed on the polished specimens using a Wolpert PW30 notched hammer.

2.4.3 Wear Resistance. The impact and wear specimens are manufactured from the same circular knife. Wear resistance was tested using the Rubber Wheel. The test procedure is in

accordance with Procedure B of the ASTM G65 standard (normal force of 130 N, 200 rpm and a linear abrasion distance of 1436 m). In order to take into account the wear of the rubber wheel, the number of wheel revolutions has been adjusted to equal the sliding distance of a new wheel a 228.6-mm (9-in.) (Ref 11). The vertical surface of the specimen was perpendicular to the rotating rubber wheel. Sand of type F36 from Quarzwerke Frechen was sprinkled onto the contact surface of the base (rubber wheel) and the mating body (specimen). The sand flow rate was approximately $300\text{--}320 \text{ g} \times \text{min}^{-1}$. The test rig used 60 Shore A rubber on a steel wheel, which worked the abrasive into the material and created a wear mark on the specimen. The wear specimens had dimensions of $90 \times 25 \times 5$ mm and the surface were all finished with 80 grit abrasive paper as an initial condition.

The volume loss was determined from the mass loss during each test and the density (7.71 g/cm^3 (Ref 12)) of the AISI D2. The weight of the specimens were measured before and after the test using a Sartorius Competence CPA225D precision balance with $d = 0.01$ mg.

2.5 Parameters, Boundary Condition and Strategy of the Heat Treatment Optimization

The approach of the new heat treatment is to replace the current conventional industrial energy-intensive heat treatment (old HT). This conventional heat treatment currently consists of a constant high austenitizing temperature in all zones of the continuous furnace (Fig. 3), in which the circular knives are austenitized for approximately 30 minutes. However, the circular blades may sometimes deform due to significant temperature gradients in the circular blade and phase transformation during heating. The circular knives' distortion causes them to no longer lie flat on the transport rollers, resulting in the entire weight being distributed over a small area. As a result, the thermally distorted blank only makes contact with the transport rollers at a few points, leading to locally increased stresses on the ceramic transport rollers. In the worst case, this can cause failure due to fracture and production stoppage. The following production constraints shall be maintained or improved if possible:

- Reduce gas and electricity consumption per circular knife in the industrial continuous and tempering furnace.
- Achieve a circular knife hardness of 700-750 HV10 after heat treatment.
- Improve the circular knives toughness.
- Achieve equal or higher wear resistance.
- Reduce thermal deformation of the knives and resulting damage to ceramic rollers in the continuous furnace.

The approach to energy-efficient heat treatment is to adjust the heat treatment temperatures and dial their duration in consequence. Currently, the austenitizing before quenching is carried out at a temperature of $T_A > 1050^\circ\text{C}$ in order to achieve the required hardness of 700–750 HV10 after the secondary hardness maximum at the tempering temperature of 510°C . However, these knives are used in the paper manufacturing industry where high operating temperatures are not present. Therefore, the used high tempering temperature is not strictly necessary. For example, a high tempering temperature is used for hot work tool steels and high-speed steels to prevent undesirable changes in the microstructure and consequently the

mechanical properties of the tool during operation at comparatively high operating temperatures in the range of 500–600 °C (Ref 13). With the selected and established material AISI D2, the required hardness can also be achieved with a lower selected austenitizing temperature and stress-relieving tempering in a temperature range up to 250 °C. In addition, an increase in toughness can be expected in this low tempering temperature range as the tempering temperature increases because of a stress relieving of the martensitic phase.

Suitable austenitizing and tempering temperatures are initially explored. Because of distortion, an appropriate pre-heating zone must be established in the continuous industrial furnace, which requires testing in the dilatometer. The determining parameter from the material's time-temperature curve is the state of the resulting solution of the matrix before quenching. Chapter 3.1.2 provides further descriptions of the solution state of the matrix and the optimization process.

3. Results and Discussion

The results and their discussion are divided into two sections. Section 3.1 discusses the process of heat treatment optimization in the laboratory scale, while section 3.2 shows the results after the industrial execution and a comparison of the mechanical properties between the conventional and the new heat treatment conditions is shown. The required energy consumption of the industrial heat treatment is also compared.

3.1 Heat Treatment Parameters Optimization—Laboratory Execution

3.1.1 Initial Condition. The initial state of the circular knives is cross-rolled strip material (AISI D2) from which the blanks are cut by laser cutting. In the standard size, the diameter is 610 mm with a thickness of 5.6 mm. The microstructure in the initial state of the AISI D2 is shown in Fig. 5. In the as-received condition, the microstructure consists of a soft annealed ferritic matrix with different carbide types and sizes. Due to the high degree of deformation during cross-rolling, the large eutectic M_7C_3 carbides with a amount of 10.5 ± 0.3 vol% are broken up ($d = 3\text{--}25 \mu\text{m}$) and distributed somewhat more

homogeneously, but the linear accumulation of these carbides still clearly indicates the primary rolling direction (Fig. 5a). These carbide bands are expected to result in anisotropic mechanical properties, particularly regarding toughness. In addition to the eutectic M_7C_3 carbides, dispersed secondary M_7C_3 carbides up to $3 \mu\text{m}$ in diameter can be detected (5.1 ± 0.1 vol.%). Also, a very small, barely detectable fraction of 0.1 vol.% MC (VC) carbides (Fig. 5b) can be found.

3.1.2 New Heat Treatment Parameters. Using the approach mentioned in section 2.5, the influence of different austenitizing temperatures at a constant holding time in the furnace of $t_A = 30$ min on the hardness and retained austenite content in the laboratory furnace was studied (Fig. 6a). Initially, the hardness increases with increasing austenitizing temperature. At the hardening temperatures between $T_A = 990\text{--}1020$ °C, a maximum hardness of about 860 HV10 is reached. With higher austenitizing temperatures, more C-rich carbides (M_7C_3 and MC) dissolve prior to quenching. This leads to greater distortion and eventually higher hardness of the martensitic microstructure as the C content in the matrix increases (Ref 14, 15). However, with increasing amounts of alloying elements in the matrix that are bound in the carbides, such as C, Cr, V, both the start (M_s) and the finish (M_f) of the martensitic transformation are shifted to lower temperatures (Ref 16). When the M_f temperature falls below the quenching temperature, the soft retained austenite remains in the microstructure, reducing the macroscopic hardness as the content increases (Ref 17). Due to the opposite properties after hardening, the martensitic hardness and the retained austenite content increase with increasing hardening temperature, resulting in the mechanical hardness plateau.

Figure 6(b) shows the hardness results for all different initial conditions (T_A) when the tempering temperature is increased in a range up to $T_{\text{Temp}} \leq 240$ °C. As the tempering temperature increases, the tetragonal distorted martensite transforms into a bcc martensite and the distorted lattice increasingly relaxes and the hardness decreases (Ref 18, 19). The hardness immediately after quenching is found to decrease by a similar ratio as the tempering temperature increases. Therefore, the hardness directly after quenching, which primarily depends on the solution state of the matrix, is the essential optimization parameter of the heat treatment.

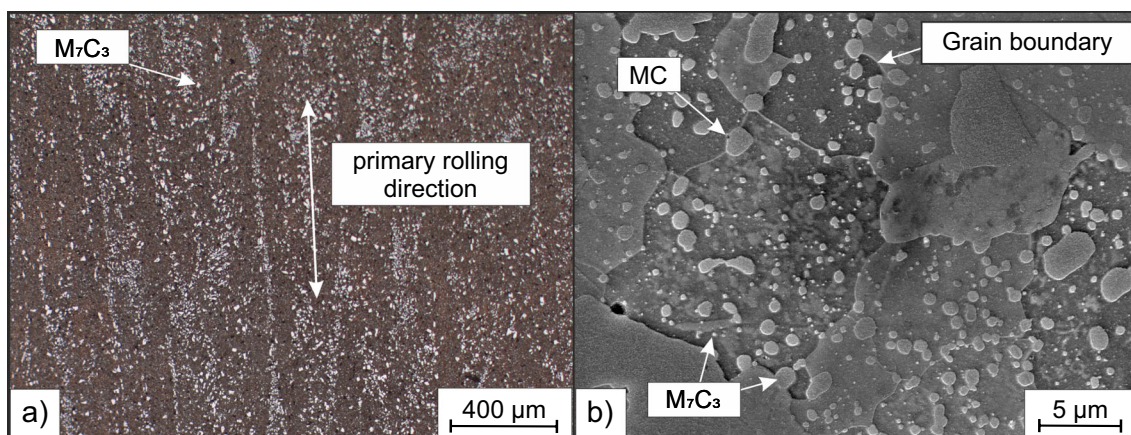


Fig. 5 Microstructure of AISI D2 in the initial state. (a) Light microscope image at 200x magnification and (b) SEM image in SE contrast and etched condition

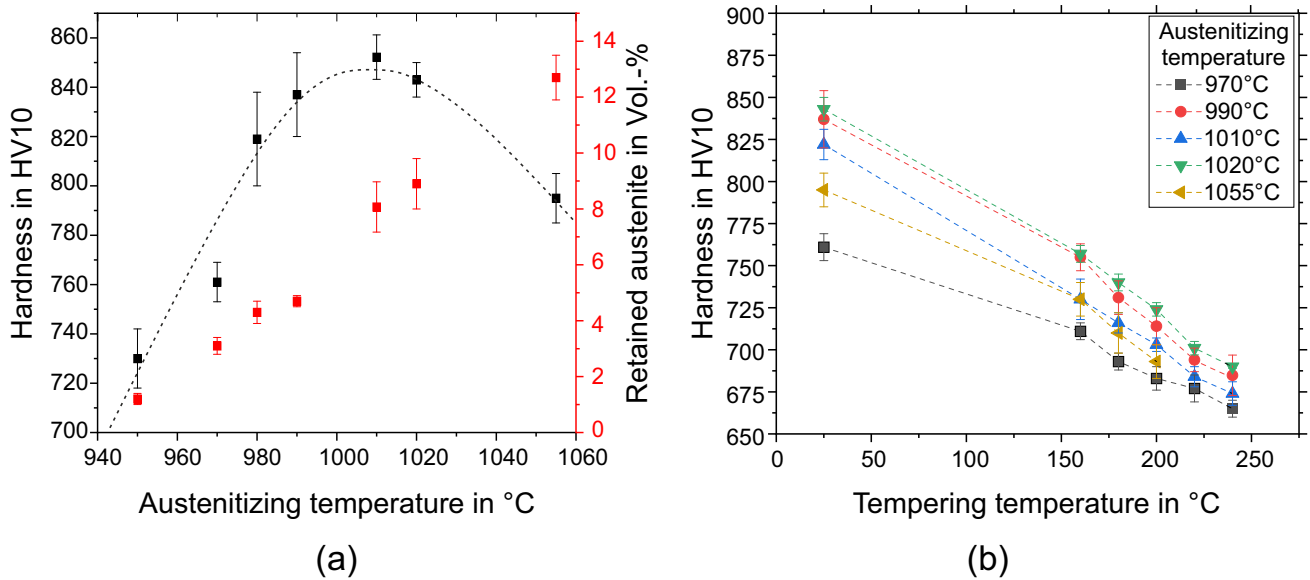


Fig. 6 Results of the heat treatment in the laboratory furnace. (a) Hardness and retained austenite after different austenitizing temperatures ($T_A = 950\text{--}1055\text{ }^\circ\text{C}$) with an identical austenitizing time of $t_A = 30\text{ min}$. (b) Results of the hardness for the different initial conditions (T_A) with increasing the tempering temperature

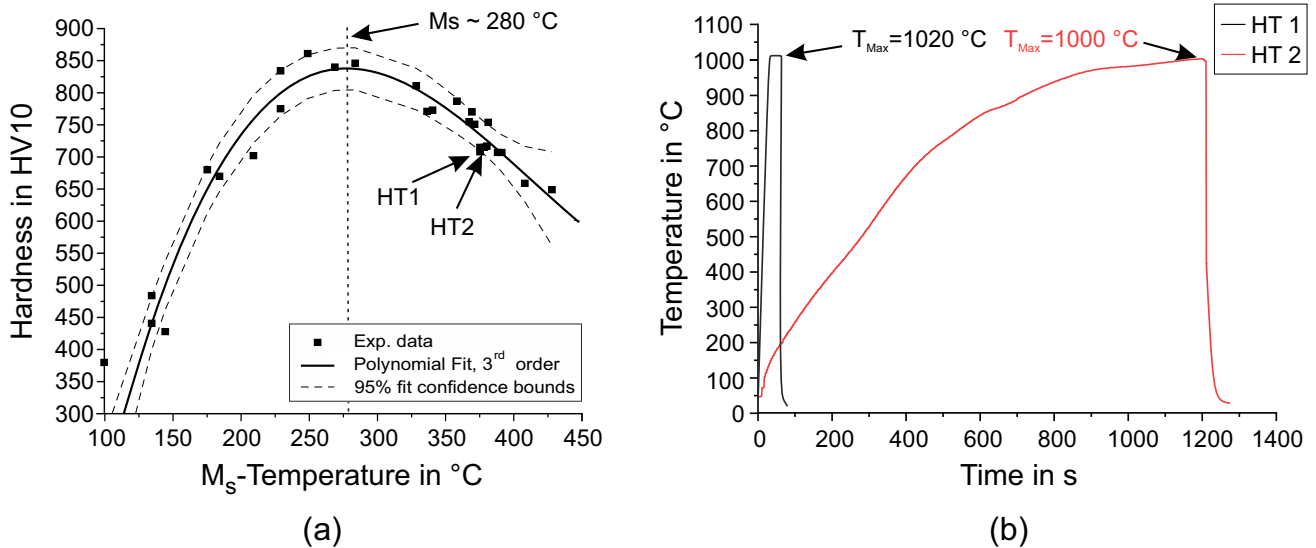


Fig. 7 Experimental results as a function of M_s temperature after heat treatment in the dilatometer with different austenitizing temperatures ($T_A = 980\text{--}1100\text{ }^\circ\text{C}$) and holding times ($t_A = 1\text{--}60\text{ min}$) (a), as well as two exemplary heat treatments with significantly different time-temperature curves (b), but with almost the same M_s temperature and the same hardness

As described above, the resulting microstructure and macroscopic hardness depend in part on the amount of alloying elements dissolved in the matrix prior to quenching (Ref 20, 21). However, the solution state of the matrix depends not only on the austenitizing temperature, as previously shown, but also on the austenitizing time. This relationship was demonstrated in previous work by Schuppener et al. for the AISI D2 (Ref 21). These carbide-rich systems require time to dissolve due to diffusion processes (Ref 22). To demonstrate the impact of the matrix solution state, which is dependent on temperature and time, Fig. 7(a) shows the hardness as a function of the M_s temperature after heat treatments in the dilatometer with different austenitizing temperatures ($T_A = 980\text{--}1100\text{ }^\circ\text{C}$) and

holding times ($t_A = 1\text{--}60\text{ min}$). In this case, the M_s temperature is used as a measurable parameter for the state of solution of the metallic matrix. To determine the maximum hardness as a function of M_s temperature from the experimental data, a third-degree polynomial fit was performed along with a 95% confidence interval. In Fig. 7(b), two exemplary heat treatments (HT1 and HT2) are shown with significantly different time-temperature curves. It is shown that different heat treatments can result in the same matrix solution state (M_s temperature) and hardness after quenching (Fig. 7a). Therefore, the solution state of the matrix is the important parameter before quenching.

Therefore, in order to obtain the maximum hardness for the AISI D2 studied, a solution state of the matrix by heat treatment

should be aimed a M_s temperature in the range of $M_s = 260\text{--}280\text{ }^\circ\text{C}$.

For the following optimization of the heat treatment parameters in terms of energy efficiency, the target solution state was an M_s temperature of around $M_s = 280\text{ }^\circ\text{C}$ and a hardness of the AISI D2 after tempering of approx. 750 HV10. Due to deformation problems of the thin blanks in the industrial continuous furnace caused by too fast and uneven heating rates, a preheating zone of $T_1 = 850\text{ }^\circ\text{C}$ and $T_2 = 920\text{ }^\circ\text{C}$ was implemented for the first two segments in the industrial continuous furnace (Fig. 3). With standard throughput speed of approximately $V_1 = 350\text{ mm}\cdot\text{min}^{-1}$, this results in a heating rate of the blanks as shown in Fig. 8(a) before they are subsequently heated to the maximum austenitizing temperature. In the following first approach, the austenitizing temperature of $T_A = 1020\text{ }^\circ\text{C}$ from the hardening maximum (Fig. 6a) was selected to reduce the total heat treatment time through the required preheating zone. Another austenitizing for energy efficiency could be $T_A = 990\text{ }^\circ\text{C}$. Here, however, the circular knives would have to remain at the hardening temperature for a longer time to reach the solution state. This would be possible in a continuous furnace by reducing the throughput speed. This is not part of this work, but should be mentioned for further energy optimization of the heat treatment process.

Figure 8(a) shows the time and temperature curves in the dilatometer at various holding times ($t_A = 5\text{--}20\text{ min}$) at a maximum temperature of $T_{\text{Max}} = 1020\text{ }^\circ\text{C}$ and a similar cooling rate as the industrial quenching after austenitizing between two cooled forging dies. Table 4 displays the results of M_s temperature and the hardness in HV10 after quenching for various holding times at T_{Max} observed in the dilatometer. As the holding time at maximum temperature increases, the M_s temperature decreases from $M_s = 305\text{ }^\circ\text{C}$ ($t_{\text{Max}} = 5\text{ min}$) to $M_s = 265\text{ }^\circ\text{C}$ at the holding time of $t_{\text{Max}} = 20\text{ min}$. In addition, the hardness increases from 830 HV10 to 865 HV10 with increasing holding time. Figure 8(b) shows the results of the tempering treatments up to $T_{\text{Temp}} = 225\text{ }^\circ\text{C}$ of the different austenitizing durations. Again, the overall hardness is decreased

by a comparable factor determined by the tempering hardness right after the quenching process.

With the required target hardness of 700–750 HV10 and the newly implemented preheating range, several heat treatment options are now possible in the industrial continuous furnace. For the subsequent industrial implementation, a holding time of approximately 10 minutes at T_{Max} of $1020\text{ }^\circ\text{C}$ and a tempering temperature of $T_{\text{Temp}} = 200\text{ }^\circ\text{C}$ were selected (Fig. 8b). With this heat treatment in the dilatometer, almost the target M_s temperature of $M_s = 280\text{ }^\circ\text{C}$ was reached, and with the stress-relief tempering at $T_{\text{Temp}} = 200\text{ }^\circ\text{C}$, approximately 750 HV10 was achieved.

3.2 Industrial Execution

The newly developed heat treatment parameters at the laboratory scale were subsequently applied in industrial production. From here on out, this new development will be referred to as low-temperature heat treatment (LTHT). The required production energy was recorded, followed by the assessment and analysis of relevant mechanical properties and microstructure. This process was also carried out for conventional manufacturing (old HT), and the obtained results were compared.

3.2.1 Energy Consumption. The heat treatment parameters determined in section 3.1.2 on the laboratory scale were now transferred to industrial production. The control temperatures T1-T5 and the throughput speed of the WMU heat treatment furnace for the old HT and LTHT are shown in Table 5. The resulting time-temperature profile measured with thermocouples of the two different heat treatments are shown in Fig. 9(a). Due to the mechanical transport arm, the thermocouple cannot remain in the circular knives during the transition to contact quenching, and the drawn cooling curve is only an approximation of the start and end temperature of the circular blank and the real cooling time of $t = 150\text{ s}$.

With the preheating zone and the reduced required maximum tempering temperature, the gas consumption of the continuous furnace is reduced from approximately 23–

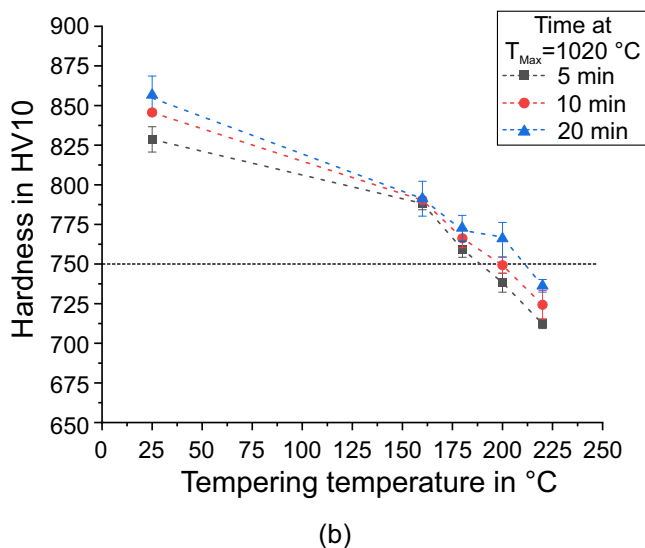
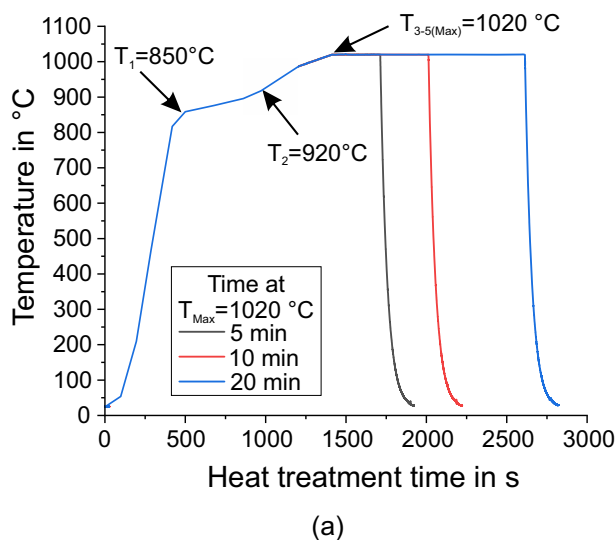


Fig. 8 Execution and results of the approach to a new developed low-temperature heat treatment (LTHT) in the dilatometer. (a) Heat treatment was conducted in the dilatometer at various holding times at a maximum temperature of $T_{\text{Max}} = 1020\text{ }^\circ\text{C}$. (b) The hardness and tempering behavior of the different holding times were evaluated up to a tempering temperature of $225\text{ }^\circ\text{C}$

Table 4 Results of the heat treatment tests in the dilatometer with identical preheating setups but different holding times at the austenitizing temperature $T_{Max} = 1020\text{ }^{\circ}\text{C}$ (Fig. 8)

Austenitizing time on $T_{Max} = 1020\text{ }^{\circ}\text{C}$ in min	5	10	20
M_s temperature in $^{\circ}\text{C}$	305 ± 5	290 ± 8	265 ± 7
Hardness after quenching ($25\text{ }^{\circ}\text{C}$) in HV10	833 ± 8	848 ± 2	865 ± 12

Table 5 Heat treatment parameters for the old conventional heat treatment (old HT) and the newly developed low-temperature heat treatment (LTHT) in the continuous furnace, along with estimated gas consumption for this setup

Heat treatment variant	Temperature in $^{\circ}\text{C}$			Throughput speed in $\text{mm}\cdot\text{min}^{-1}$		*Gas consumption in $\text{m}^3\cdot\text{h}^{-1}$
	T_1	T_2	T_3-T_5	V_1	V_2	
Old HT	1070	1070	1070	350	8500	23–24
LTHT	850	920	1020	350	8500	20–21

*Estimated average consumption by furnace manufacturer.

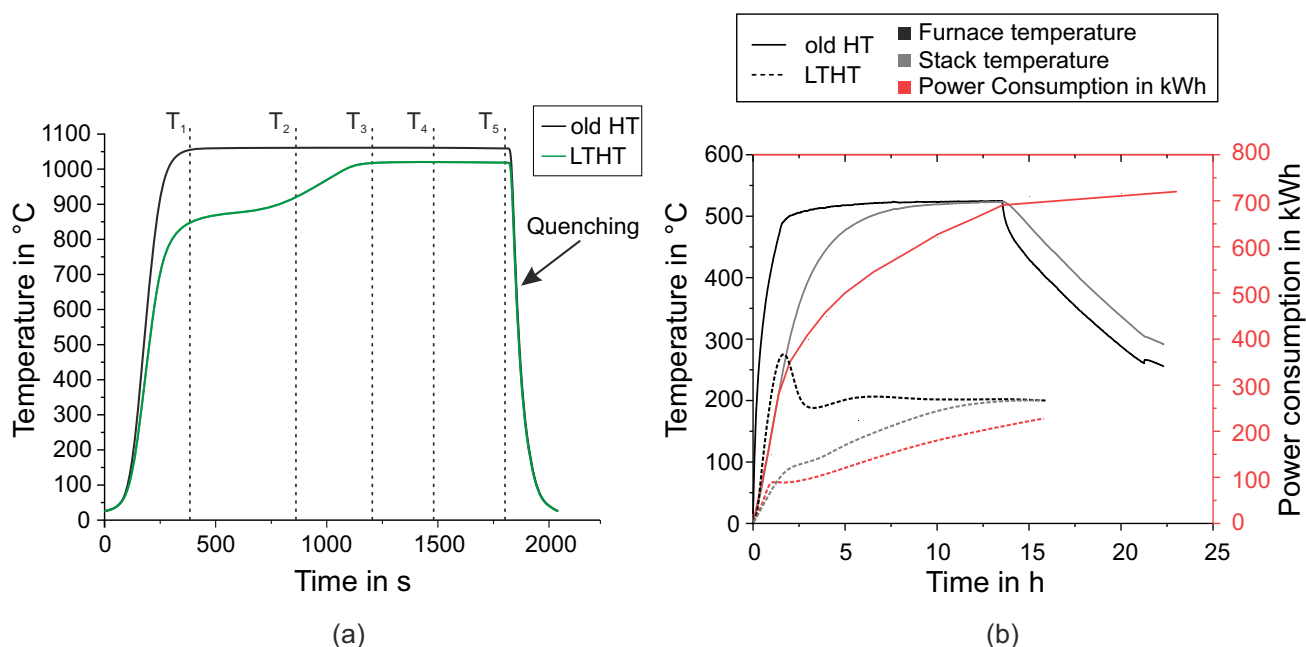


Fig. 9 Comparison of the old conventional heat treatment (old HT) and the newly developed low-temperature heat treatment (LTHT) in industrial production. Time-temperature curve of (a) the continuous furnace with the throughput speeds shown in Table 5 and (b) the tempering furnace additionally with the measurement of the temperature in the center of the tempering stack (Fig. 4) and the measured power consumption

$24\text{ m}^3 \times \text{h}^{-1}$ to $20\text{--}21\text{ m}^3 \times \text{h}^{-1}$. In the absence of measured data, the information provided by the furnace manufacturer was used. However, the data correlate very well with published measurements by Manatura et al. (Ref 23). They measured a gas consumption of $1230\text{ m}^3 \times \text{h}^{-1}$ at a T_{max} of $1085\text{ }^{\circ}\text{C}$ and a throughput of $3100\text{ kg} \times \text{h}^{-1}$ for an industrial gas-fired continuous furnace. For a production capacity of 48 circular knives per hour with a total weight of 576 kg (12 kg per Knife), a linear regression of these given data would yield a required heating capacity of $22.8\text{ m}^3 \times \text{h}^{-1}$. The values measured by Manatura et al. at $T_{max} = 1085\text{ }^{\circ}\text{C}$ are very close to the values estimated by the furnace manufacturer for the

TKM continuous furnace at a temperature of $1070\text{ }^{\circ}\text{C}$ and can therefore be taken as a reliable estimate.

At the same throughput speed of the circular knives, the required gas consumption is reduced by 12.5% per knife. This results in an energy consumption of approximately 4.9 kWh per circular knife (48 knives per hour) for the old HT with austenitizing at $T_{max} = 1070\text{ }^{\circ}\text{C}$, while only 4.3 kWh per circular knife is required for the new LTHT with $T_{max} = 1020\text{ }^{\circ}\text{C}$.

The temperature and energy measurements of a tempering heat treatment are shown in Fig. 9(b). It can be seen that for both the old HT and the LTHT, the core of the circular knife stacks takes considerably longer to reach the set tempering

temperature than the furnace itself. The maximum tempering temperature of 510 °C is reached by the tempering furnace after approximately 6 hours, while the core takes a total of 12.5 hours to reach the tempering temperature. In the case of the LTHT ($T_{\text{Temp}} = 200$ °C), the stack even needs about 14 hours to reach the furnace temperature. This is due to the very large metallic volume of each stack that needs to be heated to the furnace temperature. On the other hand, there is a 20–40 μm thick oxide layer on the surface of the circular knives after the continuous furnace, which is not removed after the individual heat treatment steps and acts as a heat transfer inhibitor between the individual circular knives in the tempering stack. As can be seen in Fig. 10, this oxide layer consists of an outer thick iron oxide layer (EDX1 + EDX2 in Table 6) and a smaller iron- and chromium-rich oxide layer (EDX3 in Table 6) on top of the tool steel. At room temperature, G. Slack (Ref 24) measured the thermal conductivity of Fe_3O_4 to be approximately $4 \text{ Wm}^{-1} \text{ K}^{-1}$. The Fe_3O_4 correlates with the chemical composition of the outer oxide layer. Schuppener et al. (Ref 12) measured a thermal conductivity for the AISI D2 at room temperature of $16 \text{ Wm}^{-1} \text{ K}^{-1}$ that was a factor of 4 higher than the oxide. In addition, G. Slack detects a decreasing thermal conductivity with increasing temperature for the Fe-Oxide, while the thermal conductivity of the AISI D2 at room temperature ($16 \text{ Wm}^{-1} \text{ K}^{-1}$) increases to about $23 \text{ Wm}^{-1} \text{ K}^{-1}$ up to 510 °C, thus increasing the difference between the tool steel and the oxide layer. In addition, M. Li et al. (Ref 25) have shown that the multilayered scale oxide layers ($\text{FeO} + \text{Fe}_3\text{O}_4$) present here have an even lower thermal conductivity of less than $2 \text{ Wm}^{-1} \text{ K}^{-1}$ at room temperature. As a result, the oxide layer reduces heat transfer between the individual circular knives and extends the required heat treatment time for all tempering heat treatments.

Since the tempering furnaces used are convection furnaces, they may be opened and shut down at a maximum temperature of approximately 300 °C to avoid possible damage to the furnace. For this reason, the high tempering temperature results in continuous circulation of the furnace temperature and thus continuous power consumption, while the furnace can be opened immediately after the LTHT. As a result, the total tempering time for the old HT is about 22.5 hours with a power consumption of about 720 kWh, while with the LTHT in the same tempering furnace, only about 225 kWh is consumed and the tempering step lasts only 16 hours.

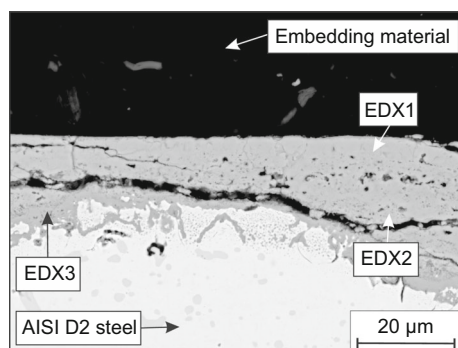


Fig. 10 SEM images of the oxide layer after industrial heat treatment in the continuous furnace ($T_{\text{max}} = 1070$ °C for 30 min and contact quenching, section 2.2.3). Cross section in X-direction Fig. 1, BSE contrast and polished condition

This results in an energy consumption of 7.2 kWh per circular knife ($n = 300$ per furnace) for a conventional three-time tempering at a temperature of 510 °C, whereas only 0.75 kWh per circular blade is required for a single relaxed tempering in the LTHT (Table 7). As a result, the new tempering heat treatment is accompanied by an almost 90% reduction in the required electricity power consumption.

3.2.2 Microstructure, Mechanical Properties, and Abrasion Wear Resistance. SEM images for the two heat treatments, old HT and LTHT, after industrial production are shown in Fig. 11, while Fig. 12 displays the EBSD analysis. The microstructure after the conventional heat treatment of austenitizing at about 1070 °C followed by three tempering steps at 510 °C consists of a high tempered bcc martensitic matrix with large eutectic and smaller round secondary M_7C_3 carbides (12.6 ± 0.4 vol.%) as well as a high number of about 100 nm small tempering carbides. The tempering temperature of 510 °C results in a bcc matrix with minimal dislocations and resulting low residual stress. This is reflected in the brightness of the band contrast in Fig. 12(c), which indicates the quality of the Kikuchi pattern. The Kikuchi pattern quality decreases as the dislocation density increases. (Ref 26, 27). The martensitic microstructure after hardening, as well as the grain orientation in the IPF-Y direction (Fig. 12e, f) show no discernible differences between the two heat treatments shown. The small size of the fine tempering carbides that precipitate during tempering makes them undetectable by x-ray quantification and EDX measurements. The EBSD analysis reveals the presence of a small amount (less than 4 vol.%) of M_2C , Fe_3C , and M_3C_2 . Gavriljuk et al. analyzed the tempering carbides of AISI D2 steel using TEM at a tempering temperature of 500 °C for 2 hours and identified them as Fe_3C (cementite) carbides (Ref 28). Singh et al. have also reported similar results after analyzing the microstructure of AISI D2 at different tempering temperatures and its abrasive wear behavior (Ref 29). In thermodynamic equilibrium calculations using the Calphad method shown by Jahazi et al. (Ref 30), Cr_3C_2 carbides are initially calculated for the selected tempering temperature. These carbides transform into M_{23}C_6 carbides after a long holding time. Due to their small size in the nanometer range, the exact determination of these carbides is not possible. Therefore, they will be referred to as tempering carbides below.

In comparison, the microstructure after the new low-temperature heat treatment consists of a stress-relieved martensitic matrix, with a higher number of dislocation density and higher residual stress (darker band contrast in Fig. 12d), with a retained austenite content of approximately 12.3 ± 0.7 vol.% as measured by XRD. Due to the lower austenitizing temperature and constant holding time selected, the total amount of M_7C_3 carbides is slightly higher than in conventional heat treatment, with a content of 13.8 ± 0.3 vol.%. Thus, even after industrial production and different heat treatments, a typical microstructure is obtained, which can also be found in the work of Gravriljuk et al. (Ref 28) and which differs mainly in the small tempering carbides (old HT) and the retained austenite content (LTHT).

A summary of all the mechanical properties determined from the industrial production is shown in Fig. 13. After both industrial heat treatments, an almost identical hardness of 720–730 HV10 is achieved, which is within the required hardness range for both heat treatments. Therefore, the main property listed in section 2.5 was satisfied. In both LTHT and conventional heat treatment, the longitudinal direction achieves

Table 6 Chemical composition of the oxides in Fig. 10 as determined by energy-dispersive x-ray spectroscopy (EDS), with values reported in atomic percent (at.%)

Element	O	Al	Si	V	Cr	Mn	Fe	Ni	Mo
EDX1	54.38	0.01	0.3	0.39	5.32	0.54	38.96	0.04	0.06
EDX2	52.62	0.04	1.16	0.85	9.80	0.56	34.24	0.12	0.59
EDX3	49.51	0.16	1.34	1.15	21.41	0.43	25.72	0.05	0.21

Table 7 Heat treatment parameters for the old conventional heat treatment (old HT) and the newly developed low-temperature heat treatment (LTHT) in the tempering furnace, along with measured power consumption per knife

Heat treatment variant	Temperature T_{Max} in °C	Electricity consumption (Per knife) in kWh
Old HT	510	7.2
LTHT	200	0.75

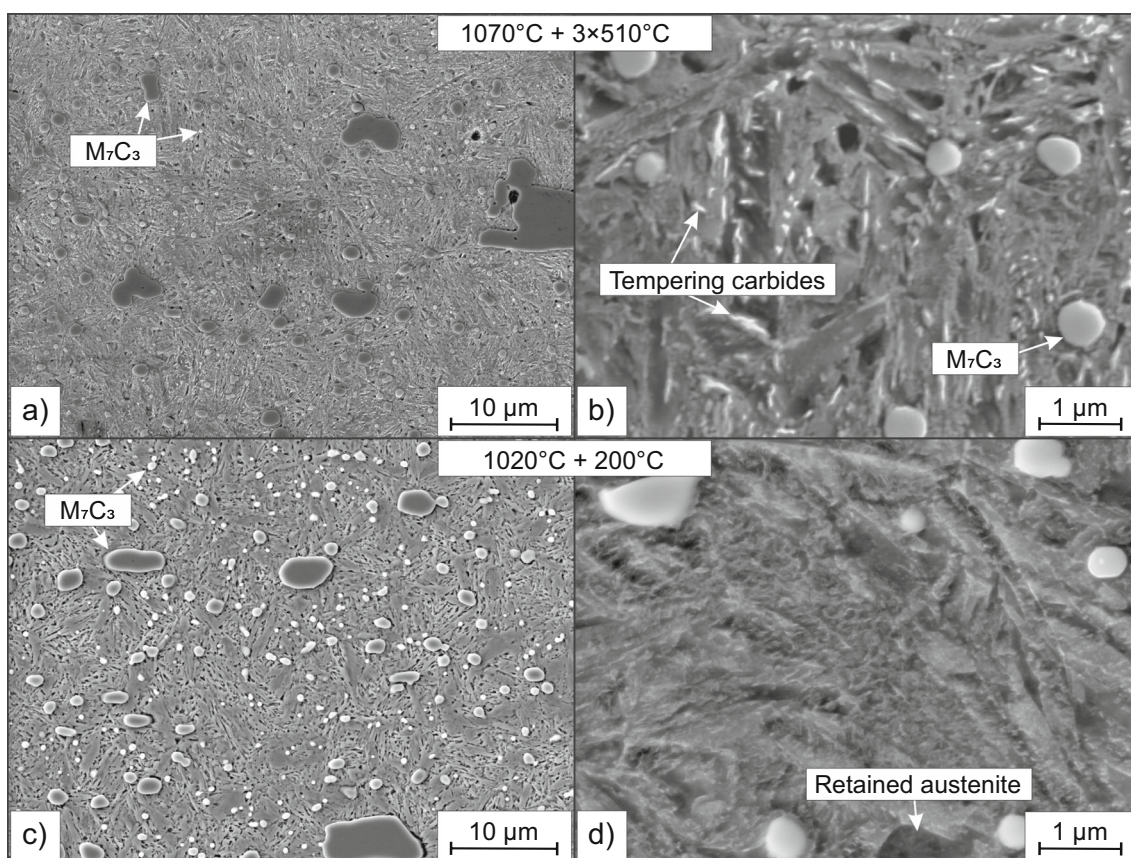


Fig. 11 SEM images of the two different microstructures after industrial heat treatment in continuous furnace and stacked tempering. SE contrast and etched condition. (a) & (b) conventional heat treatment (old HT) = 1070 °C + 3 × 510 °C and (c) & (d) low-temperature heat treatment (LTHT) = 1020 °C + 200 °C

higher toughness than the transverse direction of the impact bend specimens. Brackmann et al. (Ref 31) showed that in several tool steels, including the AISI D2, a crack can propagate more easily along the carbide-matrix interface than through the metal matrix. And, due to the primary rolling direction of the starting material, there is a linear accumulation of eutectic carbides in the rolling direction (Fig. 5) through

which the crack can travel much more easily in the transverse direction than in the longitudinal direction. As a result, the required impact energy is reduced with a lower free matrix displacement in the transverse direction. However, the LTHT variant with approximately 10 J (transverse) and 15 J (longitudinal) shows significantly higher toughness values than the conventionally produced specimens with approximately 7 J in

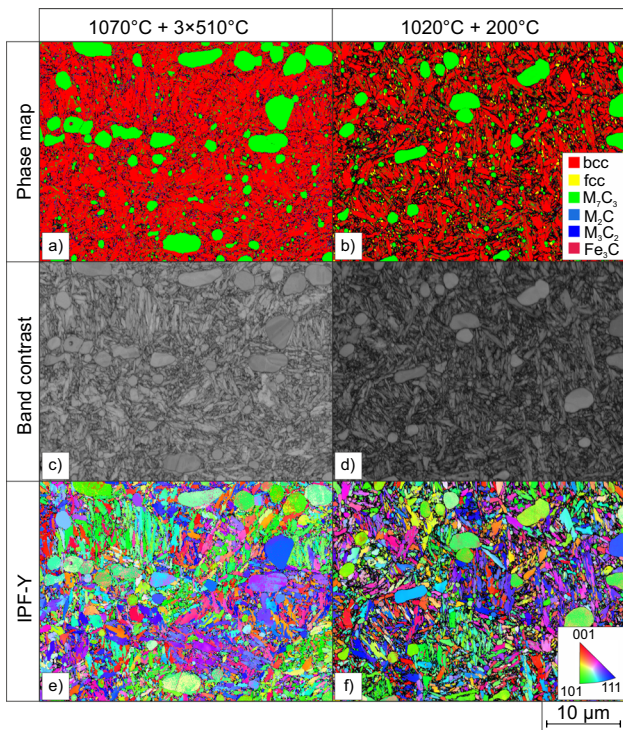


Fig. 12 EBSD images of the AISI D2 after the old heat treatment (1070 °C + 3 × 510 °C) and the optimized LTHT (1020 °C + 200 °C). (a) and (b) show the phase distribution map, (c) and (d) visualize the band contrast and (e) and (f) show the inverse pole figure (IPF-Y)

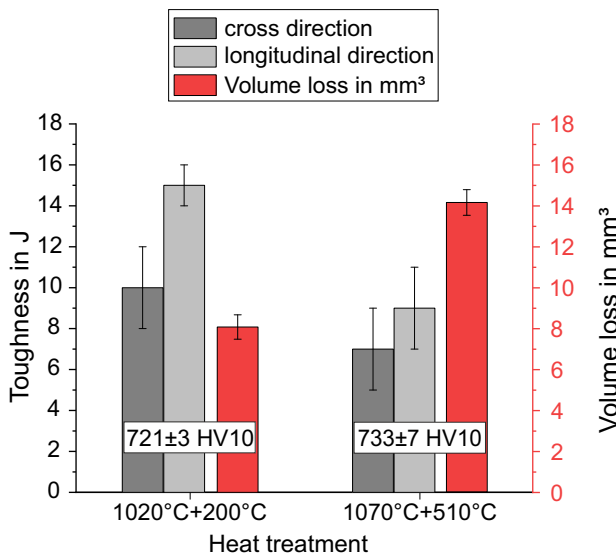


Fig. 13 Results of hardness, toughness and wear resistance tests for both heat treatment conditions after industrial production

the transverse direction and approximately 9 J in the longitudinal direction. Also in the abrasive wear tests, the LTHT variant with only 8 mm³ volume loss shows a significantly higher wear resistance than the conventionally produced specimen with a volume loss of approx. 14 mm³. Since the macroscopic hardness of the two specimens is almost identical, this parameter, which often interacts with toughness and wear

resistance in the literature, cannot be the reason. Therefore, the different mechanical properties must be related to the different microstructures, i.e., the tempering carbides (old HT) and the retained austenite (LTHT). Figure 14 displays the typical worn surface of the different heat treatment conditions, revealing the presence of both microcutting and microploughing (Ref 32). There is no significant difference in the wear track visible between both conditions.

In the wear track of the LTHT condition, as measured by x-ray, the retained austenite content decreases from 12.3 ± 0.7 vol% in the initial polished condition to an amount of approximately 8.5 ± 1.2 vol%. Silva et al. (Ref 33) have investigated the influence of the retained austenite content in carburized steels and Colaço et al. (Ref 34) in tool steels. Both found a positive influence of retained austenite microstructure on the wear resistance of the alloys. Colaço et al. explain the positive influence on wear resistance with the stress-induced transformation of metastable austenite into martensite. This phase transformation generates compressive residual stresses in the wear track and locally creates very hard new formed martensite. These literature results correlate very well with the higher wear resistance of the LTHT variant with retained austenite and the wear induced phase transformation detected by XRD.

3.2.3 Process Stability. In addition to the general mechanical properties that must be maintained for the product to be manufactured, it is important for production and product quality that the properties remain constant even if the initial conditions change slightly. One practical examples is given below.

Slight temperature variations may occur during the heat treatment process, e.g., the set tempering temperature may not be fully reached or may be slightly exceeded. For the two austenitizing temperatures $T_A = 1020$ °C and $T_A = 1070$ °C, the influence of different tempering temperature of ± 5 °C has been analyzed. The applied heat treatment parameters are shown in Table 8. The statistical evaluation of the hardness after the applied tempering variation of ± 5 °C is shown in Fig. 15(a). It can be seen that for the LTHT variant ($T_{temp} = 200$ °C), a variation of the tempering temperature of ± 5 °C has an impact on the resulting hardness of about ± 10 HV10, whereas the same variation of the tempering temperature of ± 5 °C around the tempering temperature of $T_{temp} = 510$ °C (old HT) has a significantly higher impact on the resulting hardness of about ± 20 HV10. The reason for this is that at the low tempering temperature, it is primarily the martensitic matrix that is more or less relaxed, and thus the hardness changes only slightly (Ref 35), which is evident from the low slope of the tempering curve in this temperature range of 200 °C. This can also be seen in the results of the hardness tempering behavior for the conventional and low-temperature austenitizing heat treatment which are presented in Fig. 15(b). At the high tempering temperatures, the tempering process is primarily based on the precipitation hardening through tempering carbides. However, these are only effective up to a certain size (Ref 36), and if the tempering temperature is exceeded by only a few degrees, the high temperature causes diffusion processes to accelerate, and smaller carbides dissolve in favor of larger carbides through a process known as Ostwald ripening (Ref 37). This occurs to reduce the total thermodynamically energy of the system (Ref 38), but reduces the effectiveness of particle strengthen.

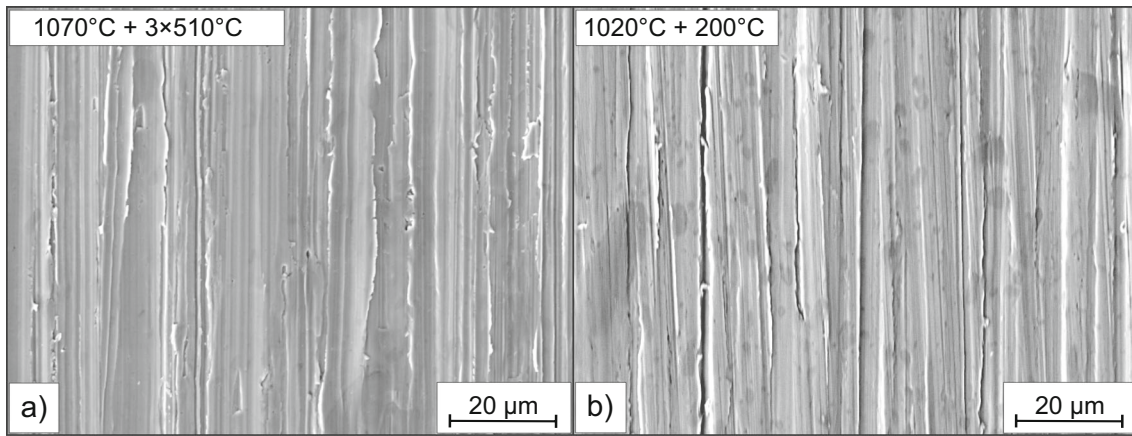


Fig. 14 SEM image of the metallic specimen after the ASTM G65 Rubber Wheel test in the wear track. (a) Conventional heat treatment and (b) the optimized LTHT

Table 8 Heat treatment parameters applied on the sample (Table 1) to investigate the influence of varying tempering temperatures

Heat treatment variant	Tempering temperature in °C		
LTHT	195	200	205
Old HT	505	510	515

Tempering temperatures of 195–205 °C were performed once, and samples in the temperature range of 505–515 °C were tempered three times.

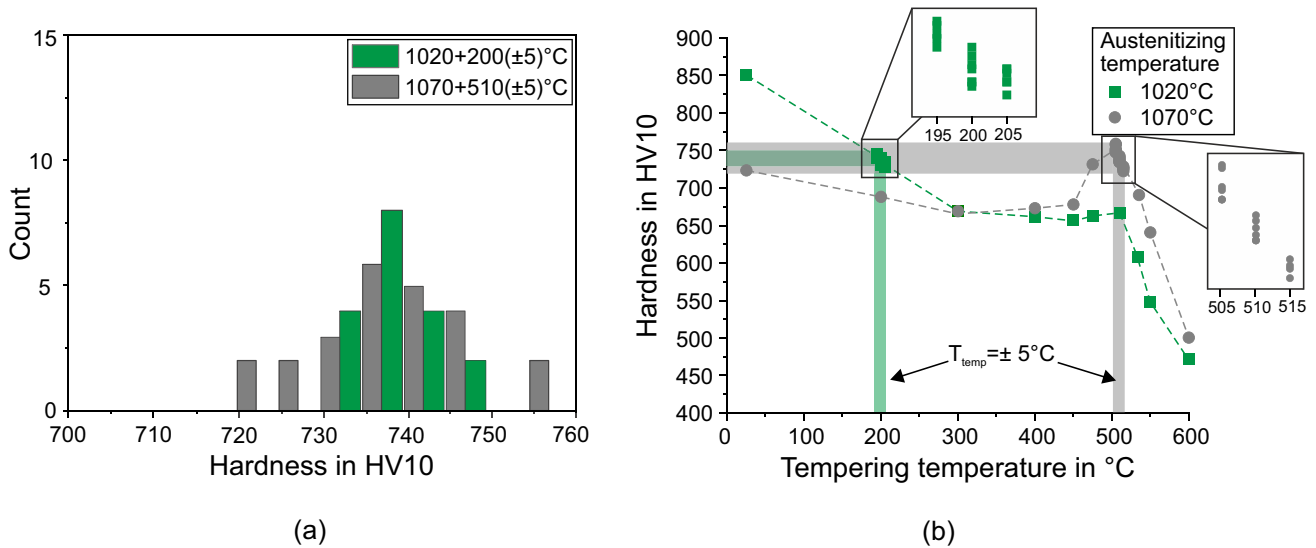


Fig. 15 Results of the hardness for the conventional and low-temperature energy-efficient heat treatment in laboratory scale. (a) Statistical evaluation of slight temperature variations in the tempering furnace (Table 8) and (b) results of the tempering behavior

4. Conclusion and Outlook

The adapted low-temperature heat treatment developed on a laboratory scale and implemented for the first time in industrial production shows promising results.

Compared to the old conventional production, the required gas consumption was reduced by 12.5% and the electrical power consumption was reduced by 90% per circular knife

during heat treatment. As a result, the total energy required for heat treatment can be reduced from 12.5 kWh to 5.1 kWh per knife. The required hardness of 700-750 HV10 can be achieved with these LTHT parameters. When tempered at slight various temperatures, the LTHT showed a significantly lower effect on hardness compared to conventional production and therefore has a wider tempering temperature range of $T_{temp} \pm 20^\circ\text{C}$ with still comparatively consistent mechanical properties. This makes it more reliable for process and quality control.

For the same hardness, both the toughness and the abrasive wear resistance of the material are improved, which is positive for the cutting application of paper articles. This improvement was related to the ductile and under wear transforming retained austenite. In addition, it was mentioned that removing the insulating oxide layer after hardening in the continuous furnace and before the tempering heat treatments could possibly further reduce the required tempering time and thus the power consumption of the tempering heat treatments. However, surface grinding prior to tempering could cause unwanted distortion of the circular blades and must be considered and investigated. After the heat treatment, grinding operations are required in the production of circular knives to produce the finished product. If the wear resistance of the material is increased, this could lead to longer processing times per knife and higher wear of the grindstone. Since only a reduction in the energy consumption of the entire production is beneficial, a complete batch of 300 circular knives will be produced with the new heat treatment parameters and the influence on the further processing steps will be analyzed and determined.

Acknowledgments

The authors would like to express their gratitude to TKM GmbH for providing the employed material and the industrial execution of the heat treatment used in this study. We would also like to thank the furnace manufacturer, WMU Wärmebehandlungsanlagen für Industrie und Umwelttechnik GmbH, for estimating the corresponding gas consumption.

Author Contributions

All authors contributed to the study conception and design. Material preparation, data collection and analysis were performed by Jannik Schuppener. The first draft of the manuscript was written by Jannik Schuppener and all authors commented on previous versions of the manuscript. All authors read and approved the final manuscript.

Funding

Open Access funding enabled and organized by Projekt DEAL. The laboratory investigations were performed at Ruhr-Universität Bochum (Bochum, Germany) and the industrial production was done at TKM GmbH (Remscheid, Germany) within the research project "KnowDiPro" funded by Arnsberg District Government as part of the Progres.NRW (ref. no. 3326010031).

Conflict of interest

The authors have no relevant financial or non-financial interests to disclose.

Open Access

This article is licensed under a Creative Commons Attribution 4.0 International License, which permits use, sharing, adaptation, distribution and reproduction in any medium or format, as long as you give appropriate credit to the original author(s) and the source, provide a link to the Creative Commons licence, and indicate if

changes were made. The images or other third party material in this article are included in the article's Creative Commons licence, unless indicated otherwise in a credit line to the material. If material is not included in the article's Creative Commons licence and your intended use is not permitted by statutory regulation or exceeds the permitted use, you will need to obtain permission directly from the copyright holder. To view a copy of this licence, visit <http://creativecommons.org/licenses/by/4.0/>.

References

1. H. Berns and W. Theisen, *Ferrous Materials: Steel and Cast Iron*, Springer, Berlin, Heidelberg, 2008
2. E. Hornbogen, H. Warlimont and B. Skrotzki, *Metalle: Struktur und Eigenschaften der Metalle und Legierungen*, 7th ed. Springer, Berlin, Heidelberg, 2019
3. H.K.D.H. Bhadeshia, R.W.K. Honeycombe, *Steels: Microstructure and properties*, Fourth edition, Elsevier Butterworth-Heinemann, Amsterdam, Boston, Heidelberg, London, New York, Oxford, Paris, San Diego, San Francisco, Singapore, Sydney, Tokyo (2017)
4. S. Hu, L. Zhu, M. Zhang, X. Tang and X. Wang, Development and Prospect of Vacuum High-Pressure Gas Quenching Technology, *Materials (Basel, Switzerland)*, 2023, **16**, p 7413.
5. S. Andreev, System of Energy-Saving Optimal Control of Metal Heating Process in Heat Treatment Furnaces of Rolling Mills, *Machines*, 2019, **7**, p 60.
6. Information on <https://www.tkmgroup.com/de/logsaw-papierkreissmesser>
7. J. Schindelin, I. Arganda-Carreras, E. Frise, V. Kaynig, M. Longair, T. Pietzsch, S. Preibisch, C. Rueden, S. Saalfeld, B. Schmid, J.-Y. Tinevez, D.J. White, V. Hartenstein, K. Eliceiri, P. Tomancak and A. Cardona, Fiji: An Open-Source Platform for Biological-Image Analysis, *Nat. Methods*, 2012, **9**, p 676–682.
8. S. Benito, N. Wulbieter, F. Pöhl and W. Theisen, Microstructural Analysis of Powder Metallurgy Tool Steels in the Context of Abrasive Wear Behavior: A New Computerized Approach to Stereology, *J. Mater. Eng. Perform.*, 2019, **28**, p 2919–2936.
9. ASTM, Standard practice for X-ray determination of retained austenite in steel with near random crystallographic orientation, E975-13
10. DIN-Normenausschuss Materialprüfung (NMP), Metallic materials—Charpy pendulum impact test: Part 1: Test method (ISO 148-1:2016); German version EN ISO 148-1:2016, Beuth Verlag GmbH, Berlin, Heidelberg (2016)
11. ASTM International, Standard Test Method for Measuring Abrasion Using the Dry Sand/Rubber Wheel Apparatus: Designation: G 65—00, ASTM G65–91, ASTM, United states, West Conshohocken
12. J. Schuppener, A. Berger, S. Benito and S. Weber, Simulation of Local Metastable Microstructural States in Large Tools: Construction and Validation of the Model, *Int. J. Adv. Manuf. Technol.*, 2023, **128**, p 4235–4252.
13. H. Berns (Ed.), *Hartlegierungen und Hartverbundwerkstoffe: Gefüge, Eigenschaften, Bearbeitung, Anwendung*, Springer Berlin Heidelberg, Berlin, Heidelberg, s.l. (1998)
14. J. Mola and M. Ren, On the Hardness of High Carbon Ferrous Martensite, *IOP Conf. Ser.: Mater. Sci. Eng.*, 2018, **373**, p 12004.
15. J. Damon, S. Dietrich and V. Schulze, Implications of Carbon, Nitrogen and Porosity on the $\gamma \rightarrow \alpha'$ Martensite Phase Transformation and Resulting Hardness in PM-Steel Aсталoy 85Mo, *J. Market. Res.*, 2020, **9**, p 8245–8257.
16. J. Platl, H. Leitner, C. Turk and R. Schnitzer, Determination of Martensite Start Temperature of High-Speed Steels Based on Thermodynamic Calculations, *Steel Res. Int.*, 2020, **91**, p 2000063.
17. Y.Y. Su, L.H. Chiu, T.L. Chuang, C.L. Huang, C.Y. Wu and K.C. Liao, Retained Austenite Amount Determination Comparison in JIS SKD11 Steel Using Quantitative Metallography and X-Ray Diffraction Methods, *Adv. Compos. Mater.*, 2012, **482–484**, p 1165–1168.
18. G. Krauss and A.R. Marder, The morphology of martensite in iron alloys, *Metall. Trans.*, 1971, **2**, p 2343–2357.
19. G. Nolze, A. Winkelmann, G. Cios and T. Tokarski, Tetragonality Mapping of Martensite in a High-Carbon Steel by EBSD, *Mater Charact.*, 2021, **175**, 111040

20. S. van Bohemen, Bainite and Martensite Start Temperature Calculated with Exponential Carbon Dependence, *Mater. Sci. Technol.*, 2012, **28**, p 487–495.
21. J. Schuppener, S. Müller, S. Benito and S. Weber, Short-Term Heat Treatment of the High-Alloy Cold-Work Tool Steel X153CrMoV12: Calculation of Metastable Microstructural States, *Steel Res. Int.*, 2022, **94**, p 2200452.
22. F. Su, H. Wang and Z. Wen, Modeling and Simulation of Dissolution Process of Bulk Carbide in Fe–1C–1.44Cr Low-Alloy Steel, *J. Mater. Res. Technol.*, 2021, **11**, p 992–999.
23. K. Manatura, M. Tangtrakul, A Study of Specific Energy Consumption in Reheating Furnace Using // A Study of Specific Energy Consumption in Reheating Furnace Using Regenerative Burners Combined with Recuperator. 2, 4, Silpakorn Univ. Sci. Technol. J. 7–13 (2010)
24. G.A. Slack, Thermal Conductivity of MgO, Al₂O₃, MgAl₂O₄, and Fe₃O₄ Crystals 3° to 300 °K, *Phys. Rev.* 427 (1962)
25. M. Li, R. Endo, M. Akoshima, H. Tanei, H. Okada and M. Susa, Thermal Conductivity of Oxide Scale Thermally Grown on Iron Substrate Corrected by Temperature-dependent Interfacial Thermal Resistance in Laser Flash Measurement, *ISIJ Int.*, 2019, **59**, p 398–403.
26. S. Zaeferrer, P. Romano and F. Friedel, EBSD as a Tool to Identify and Quantify Bainite and Ferrite in Low-Alloyed Al-TRIP Steels, The Royal Microscopical Society, *J. Microscopy*, 2008, **230**, p 499–508.
27. E.J. Payton, L. Agudo Jácome and G. Nolze, Phase Identification by Image Processing of EBSD Patterns, *Microsc. Microanal.*, 2013, **19**, p 842–843.
28. V.G. Gavriljuk, V.A. Sirosh, Y.N. Petrov, A.I. Tyshchenko, W. Theisen and A. Kortmann, Carbide Precipitation During Tempering of a Tool Steel Subjected to Deep Cryogenic Treatment, *Metall. Mat. Trans. A*, 2014, **45**, p 2453–2465.
29. K. Singh, R.K. Khatirkar and S.G. Sapate, Microstructure Evolution and Abrasive Wear Behavior of D2 Steel, *Wear*, 2015, **328–329**, p 206–216.
30. H. Ghasemi-Nanesa and M. Jahazi, Simultaneous Enhancement of Strength and Ductility in Cryogenically Treated AISI D2 Tool Steel, *Mater. Sci. Eng. A*, 2014, **598**, p 413–419.
31. L. Brackmann, D. Wingender, S. Weber, D. Balzani and A. Röttger, Influence of Hard Phase Size and Spacing on the Fatigue Crack Propagation in Tool Steels—Numerical Simulation and Experimental Validation, *Fatigue Fract. Eng. Mat. Struct.*, 2023, **46**, p 3872–3891.
32. K.-H. Gahr, *Microstructure and wear of materials*, Elsevier Science Publishers, Amsterdam, 1987
33. V.F. Da Silva, L.F. Canale, D. Spinelli, W.W. Bose-Filho and O.R. Crnkovic, Influence of Retained Austenite on Short Fatigue Crack Growth and Wear Resistance of Case Carburized Steel, *J. Mater. Eng. Perform.*, 1999, **8**, p 543–548.
34. R. Colaço and R. Vilar, On the Influence of Retained Austenite in the Abrasive Wear Behaviour of a Laser Surface Melted Tool Steel, *Wear*, 2005, **258**, p 225–231.
35. R.A. Grange, C.R. Hribal and L.F. Porter, Hardness of Tempered Martensite in Carbon and Low-Alloy Steels, *Metall. Trans.*, 1977, **8**, p 1775–1785.
36. W. Bochnowski, H. Leitner, L. Major, R. Ebner and B. Major, Primary and Secondary Carbides in High-Speed Steels After Conventional Heat Treatment and Laser Modification, *Mater. Chem. Phys.*, 2003, **81**, p 503–506.
37. P. Voorhees, The Theory of Ostwald Ripening, *J. Stat. Phys.*, 1985, **38**, p 231–252.
38. G. Gottstein, *Materialwissenschaft und Werkstofftechnik*, Springer, Berlin, Heidelberg, 2014

Publisher's Note Springer Nature remains neutral with regard to jurisdictional claims in published maps and institutional affiliations.